Proceedings of ASME Turbo Expo 2022
Turbomachinery Technical Conference and Exposition
GT2022
June 13-17, 2022, Rotterdam, Netherlands

GT2022-80167

NUMERICAL INVESTIGATION OF BLADELESS COMPRESSOR ON DIFFERENT DISK SPACES AND DIFFUSER CONFIGURATIONS

Ravi Nath Tiwari
University of Genoa, TPG Italy
Email: ravinath.tiwari@edu.unige.it

Konstantinos Eleftheriou
Aristotle University of Thessaloniki, Greece, Email: elefthkd@auth.gr

Mario Luigi Ferrari
University of Genoa, TPG, Italy

Theofilos Efstathiadis
Aristotle University of Thessaloniki, Greece

Alberto Traverso
University of Genoa, TPG, Italy

Anestis Kalfas
Aristotle University of Thessaloniki, Greece

ABSTRACT

The cost-effectiveness of turbomachinery is a key aspect within the small-size compressor market. For this reason, Tesla turbomachinery, invented by Nikola Tesla in 1913, could be a good solution, particularly for low volumetric flow applications, where volumetric compressors are usually used. It consists of a bladeless rotor which stands out for its ease of construction and its ability to maintain almost the same performance as size decreases. One of its advantages is that it can run either as a turbine or as a compressor with minor modifications at the stator. The objective of this paper is to investigate a 3kW Tesla compressor, which design was derived from an analogous Tesla expander prototype (59% isentropic efficiency from the numerical study), by conducting a computational fluid dynamic analysis for different disk gaps and diffuser configurations.

The potential of the Tesla compressor is shown to be quite promising, with a peak isentropic efficiency estimated at 53%. Although bladeless compressor is a simple turbomachinery device, different parts i.e., diffuser, tip clearance, and volute need to be optimized. Utilizing computational fluid dynamics algorithms, different disk gaps and different diffusers are simulated in order to increase the overall performance of the compressor and understand the flow dynamic behavior behind this technology. The dimensionless Ekman number is used to express the optimum disk space of the compressor rotor. Thus, the overall performance of the Tesla compressor is improved by 5-10% points compared to the initial model. Simultaneously, diffuser optimization strategies are applied and proved that there is a direct impact on the optimum design conditions, improving the pressure ratio at high mass flow rates.

Keywords: Tesla turbomachinery, Ekman Number, Bladeless compressor

NOMENCLATURE

p_{t1}	Inlet total pressure [Pa]
p_{t2}	Outlet total pressure [Pa]
T_{t1}	Inlet total temperature [K]
E_k	Ekman number [-]
2h	Disk gap [mm]
t	Disk thickness [mm]
r_1	Inner radius [mm]
r_2	Outer radius [mm]
k	Specific heat ratio [-]
C_p	Isobaric specific heat [kJ/(kg K)]
N	Rotational speed [krpm]
ν	Kinematic viscosity [m^2/s]
ω	Angular velocity [rad/s]
η	Efficiency [-]
Re	Reynolds number [-]
δ	Boundary layer thickness [mm]
$\dot{m}$	Mass flow rate [g/s]
τ	Torque [Nm]
P	Power [W]
α_2	Flow angle [°]
V_r	Radial velocity
V_t	Tangential velocity

Subscripts

t-t	Total to Total
st-st	Static to Static

Acronyms

CFD	Computational Fluid Dynamics
PR	Pressure Ratio

1. INTRODUCTION

The micro-scale compressor demand is increasing for microscale applications i.e. power generation, medical, chemical processes, etc. The conventional compressor performance significantly decreases with decreased size, while it is almost constant for the bladeless turbomachinery. Nikola Tesla (1856-1943) is a famous scientist whose research and inventions are studied until now. Bladeless turbomachinery is the best of his inventions, according to his interview in 1912. Tesla filed his first patent in 1909. It was a boundary layer pump which was transferring energy to the fluid through multiple flat disks using viscous forces. Based again on the same principle, he managed to patent a turbine in 1911. Both boundary layer devices were accepted in 1913 [1,2] and took the name of their inventor. Until now, they are known as Tesla turbomachinery. Although Tesla turbomachinery is a revolutionary technology, it is not commercially applied to any industrial field due to its low performance. Tesla turbines can reach up to 25% isentropic efficiency according to several experimental studies [3,4], with a peak of 36% [6], which is significantly lower than the theoretical one based on literature. However, Tesla turbomachinery has a variety of advantages such as simple design, low manufacturing cost, and the ability to run either as a turbine or as a compressor with minor changes. Furthermore, bladeless turbomachinery becomes a reasonable solution compared to conventional bladed impellers when scale-down design methods are applied [5]. This is mainly due to the constant performance of the first as size decreases. Thus, Tesla turbomachinery can be a potential prime mover for Micro Gas Turbines in the range of 200W - 3kW [6].

The concept of running a Tesla turbine in reverse mode as a Tesla compressor is investigated in this paper. Tesla compressor consists of parallel flat co-rotating disks, mounted on a single shaft with the specified gap. Around the disks, there is a casing and several diffusers. The rotor causes the flow to enter through the center of the disks and exit from the multiple diffuser channels. Different gaps between the disks will be numerically analyzed and different diffuser configurations will be assessed. In this work, the original geometry of the existing expander prototype [6] is mildly changed to optimize the reverse compressor operation.

2. STATE-OF-THE-ART

There are several aerodynamic issues when a scaled-down component is designed. High rotational speed, which is a requirement to maintain the tip Mach number constant, creates vibration problems. The boundary layer thickness is comparable to the passage dimensions of the turbomachinery, increasing blockage and, as a result, affecting the efficiency. Furthermore, the major loss mechanism in micro turbomachinery is the viscous losses which are enhanced due to low Reynolds number [8].

In the bladeless compressor, fluid viscosity is the main principle of transferring energy to the fluid [9]. The fluid is facing shear forces due to the rotation of the disk rotor and moves radially due to centrifugal forces. The fluid follows a path of an Archimedean spiral, and its size is proportional to the rotational speed. As a result, the fluid increases its total pressure while it reaches the diffuser part and then the volute.

The literature on Tesla compressors is quite limited. Generally, the first attempts were made in the direction of understanding the internal flow field. Crawford and Rice [10] found that the maximum performance of a Tesla pump occurred when the flow between the corotating disks is laminar. Boyd and Rice [11] split the flow field into two regions, the entrance, and the asymptotic/ Ekman regions. In the first one, the flow velocity profile is not fully developed while in the second one, the boundary layer is fully developed, as shown in Fig.1. Breiter and Pohlhausen [13] created a model which calculates analytically the solution of the linearized governing equations. They assumed zero normal pressure gradient on the disk and low relative velocities. The model showed that the boundary layer profile is affected by the kinematic viscosity, the angular velocity, and the distance between the disks. Laroche and Ribaud [9] defined a parameter that contains all the previous variables, and it is called Ekman Number. The complete equation of Ekman's number is given in the next section. An analytical model is also created by Rice [14] assuming a 2D flow between the disks.

Generally, these kinds of models were significantly weak to accurately estimate the flow parameters, especially in the asymptotic region. As a result, a few numerical analyses have been done in order to predict the performance of Tesla pumps and compressors. A finite difference method was applied by Boyd and Rice [11] to calculate the flow field between rotating disks, facing however issues in terms of high computational time. An integral method to define the flow parameters in the disk gap was chosen by Boyack and Rice [15]. This model had the same results as the one built by Boyd and Rice [11] with a reduced execution time. Further improvement in computational time of the integral method model was done by Crawford and Rice [10].

Aside from numerical or analytical models, bladeless compressors and pumps have also been experimentally investigated. Thus, a few experiments are conducted for corotating rotors, inlet geometries, diffusers, and volutes to assess the performance of the turbomachinery. Hasinger and Kehrt [17] tested experimentally a shear force pump. Pressure probes were used to measure the efficiency of the rotor. The model of the pump was created measuring the outlet pressure and changing rotational speed and mass flow rate. The measured efficiency was approximately 55%, lower than the one calculated using the analytical method. Rice [14] tested multiple-disk pumps and compressors. He also produced the performance map of the tested components. During his experiments, the maximum measured compressor efficiency was 21%, while the corresponding rotor efficiency predicted was 95%. Rice [18] assumed that this inconsistency was due to the diffuser configuration, something which is not confirmed yet. Almost all the bladeless pumps have been designed with simple methods based on empirical models. As a result large disk gap is implemented, leading to turbulence flow between the disk gaps [14,23].

In this paper, the performance of a bladeless turbine running in reverse mode is investigated. A University of Genova prototype 3 kW air Tesla turbine model is numerically studied as a Tesla compressor [6]. In this paper existing model consider as case 0 model and geometry details are shown in Table 1. The disk gap should be approximately twice the boundary layer thickness to maximize performance, where optimal Reynolds numbers are 5 or 6, based on Eq. 2 [18]. The Tesla rotor efficiency is determined for different disk spaces of the case 0 models, where the gap is optimized based on the Ekman number. The various cases are numerically tested using ANSYS CFD software. Table 1 shows the tested configurations, defining the four different geometrical rotor models (M1-M4).

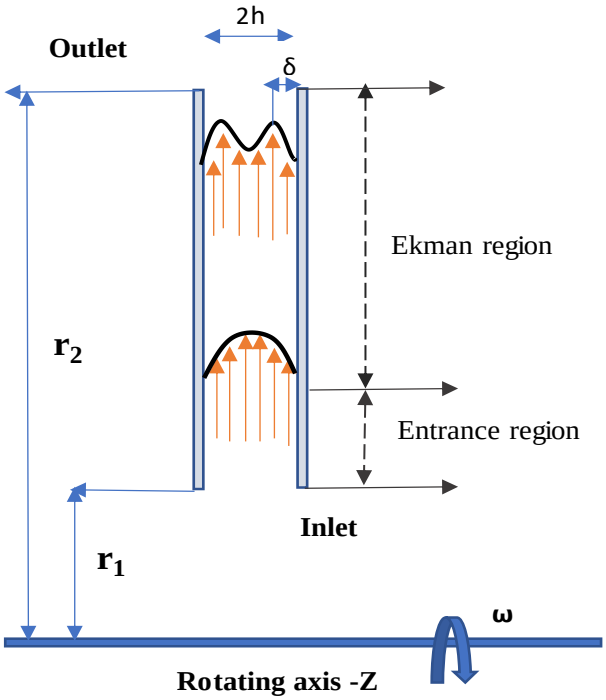

FIGURE 1: BOUNDARY LAYER PROFILES BETWEEN TWO COROTATING DISKS

TABLE 1: DESIGN PARAMETERS OF TESLA COMPRESSOR

Design Parameter	**Size**			
Model	M1	M2	M3	M4
Outer diameter (mm)	120			
Inner diameter(mm)	30			
Disks thickness(mm)	0.1			
Speed (rpm)	40000			
Resulting parameter				
Ek	0.8	1.25	1.6	2
Gap(mm)	0.1	0.15	0.2	0.25
Re number, $\omega(2h)r_1/\nu$ [12]	800	1201	1601	2001
Re number, $\omega(2h)^2/\nu$ [18,20]	2.6	6.1	10.5	16.5
Disk numbers	120	96	80	69

3. NUMERICAL METHODOLOGY

With regards to the numerical analysis, ANSYS FLUENT provided 2 types of solvers i.e., Pressure based, and density-based. The pressure-based approach was developed Initially for incompressible flow, while a density-based approach was used for the high-speed compressible flow. However, both methods have now been extended to solve a wide range of flow conditions beyond their original capability [23,25]. Pressure-based solvers have demonstrated the capability to address highly compressible flows in turbomachinery applications, providing more computational stability than density-based solvers [12,23,24]. Therefore, a pressure-based steady solver is selected to solve the steady and compressible flow, with ideal gas as a working fluid in the current study.[12]. The transition of laminar to turbulent or vice versa is not expected in the tesla rotor due to the very low Reynolds number. Moreover, the objective of the study captures the shear force in the rotor accurately. The 3D Navier-Stokes equations are solved utilizing ANSYS FLUENT and are discretized using the "Finite Volume Method". The viscous model which is utilized is k-omega SST, a turbulence model which belongs to the Reynolds-Averaged Navier-Stokes (RANS) family and becomes the current industry standard for turbulence modeling [16]. k-omega SST combines the better prediction of the k-ω the model in the near-wall region with the k-ε model advantages in the far-field [26]. The flow between rotor and stator is turbulent due to the high velocity before the diffuser inlet. In order to cater to the requirement of y+ of the rotor and diffuser inlet, the k-omega SST model is used. k-omega SST model uses the equation based on the y+ value. It also considers the energy equation in order to take into account the heat transfer in the flow field. The viscous heating option is selected to consider the temperature change resulting from shear forces.

The governing equations are discretized using second-order upwind linear interpolation and solved using the COUPLED scheme for pressure and velocity coupling in fluent [25]. In this study, the flow domain between two rotating disks is considered stationary. For the entire "compressor-diffuser" configuration, half of the disk thickness and half of the gap rotating disks ss considered as a single fluid domain shown in Figure 2. This computational approach simplifies the problem, decreasing the execution time.

The numerical results are considered to be converged when the residuals of each solved equation are lower than 10^{-6}. Furthermore, the mass flow rate is one of the convergence criteria with an acceptable variation of less than 0.5%. At the same time, different flow parameters (i.e., inlet/outlet velocity and temperature) and mechanical parameters (torque and power), as well as flow field velocity and pressure contours, are continuously monitored in order to ensure that they are getting stable as the iteration number increases.

4. TESLA ROTOR ONLY ANALYSIS

A computational fluid dynamic analysis was initially conducted in the rotor field only. This means that the numerical domain contains the area between two flat disks where the fluid governing equations are solved. The outcome of this analysis

provides useful information for rotor-only features, in particular pressure ratio, isentropic efficiency, that will later help to understand the rotor-diffuser coupled behavior.

4.1 Design Method

Table 1 shows the design parameters of the rotating disks. Based on the original prototype geometry (optimized for expander operation), the inner diameter of the compressor is 60mm and the outer is 120 mm. The geometrical parameters, as well as the flow path, are illustrated in Figure 1. Based on the literature [9,13], the main non-dimensional parameter driving the boundary layer profile and as a result, the overall performance of two corotating bladeless rotors, is the Ekman number. The Ekman number is the ratio of the half-width of disk gap h and the boundary layer thickness δ, see Eq. (1). Based on literature there are two most used Reynolds number equations as shown in Eq. (2) & (3). The first one is based on the disk gap[18,20] and the second one on the radius [12]

$$E_k = h/\delta \;=\; h\sqrt{\omega/\nu} \tag{1}$$

$$R_e = \frac{\omega(2h)^2}{\upsilon} \tag{2}$$

$$R_{e1} = \frac{\omega r_1 2h}{\upsilon} \tag{3}$$

The objective of this work is to find the optimum Ekman and Reynold number for the Tesla compressor rotor. It is already known that the best efficiency appears when the Ekman number is between 1 and 2 [9]. This is the reason why the Ekman number is chosen to be 0.8, 1.25, 1.6, and 2 for the different design models, respectively. Wang [9] chose Ekman number 2 for his analysis. The rotational speed is constant for every case in order to control Ekman number by changing the gap between the disks. Reynolds number is also calculated for the different disk space rotor models to obtain the optimal configuration. It is expected that peak efficiency is reached when Reynolds is approximately 5 or 6 (Eq. 2) [18,20]. Table 1 also shows the resulting Reynolds numbers calculated using Eq. 2 and 3. This study is focusing to define the optimal Ekman and Re numbers of the bladeless compressor.

4.2 Mesh dependency analysis and boundary conditions

The "case 0" model and proposed Tesla compressor consists of 8 diffusers; thus, a 45 deg-slice is simulated. Assuming axisymmetric flow, only half of the flow path is simulated, as shown in Figure 2. Figure 2 also depicts the boundary conditions (i.e., inlet, outlet, moving wall, and periodic boundary conditions). A hexahedron grid is generated for the independent rotor analysis and tetrahedral mesh is chosen for the bladeless "rotor-diffuser" model analysis to discretize the computational domain. Furthermore, an inflation layer of 4 cells is applied close to the stationary and rotating wall regions, in order to refine the mesh and resolve accurately the boundary layer shape. The y+ is a non-dimensional parameter that is important to see how accurately the boundary layer is resolved. Two types of walls have been considered in analysis, 1st stationary and 2nd rotating walls as shown in Fig 2. A stationary wall is considered at diffuser where the average y+ value is less than 5 and a rotating wall is consider at rotor where y + value is less than 1. In the case of the k-ω SST model, the facet average y+ value should be less than 5 is recommended for accuracy, and therefore in the current study, the average y+ value is maintained less than 5.

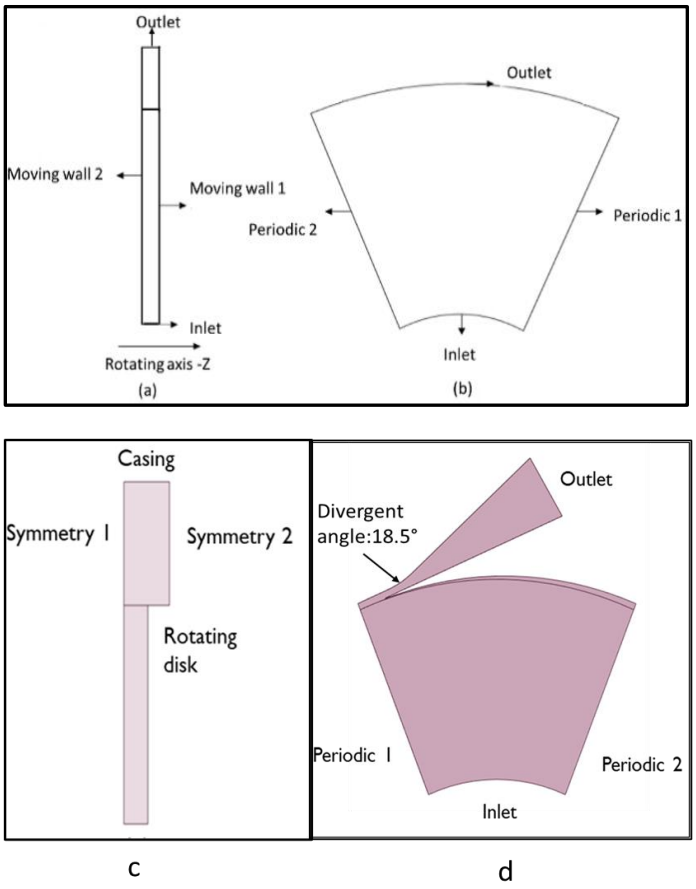

FIGURE 2: BOUNDARY CONDITIONS OF THE ROTOR ONLY AND DIFFUSER ANALYSES: (a & c) CROSS-SECTIONAL VIEW AND (b & d) FRONT VIEW

After conducting a mesh dependency analysis starting from 200,000 cells until 2,000,000 cells, an error of less than 0.1% is observed at mass flow and torque convergence (Fig. 3). Fig. 4 (a & b)shows the generated mesh of the "rotor only" and "case 0 bladeless compressor". The analysis is conducted with a mesh of 1,310,000 cells which corresponds to an error of 0.05% for torque and mass flow variables and this mesh size is selected for the present study.

The boundaries conditions at inlet/outlet are set as total pressure inlet and mass flow outlet [20]. The total pressure of 101325 kPa and total temperature of 300 K are applied at the inlet while different mass flow rates are assigned at the outlet. With regards to walls, non-slip condition and adiabatic options are selected.

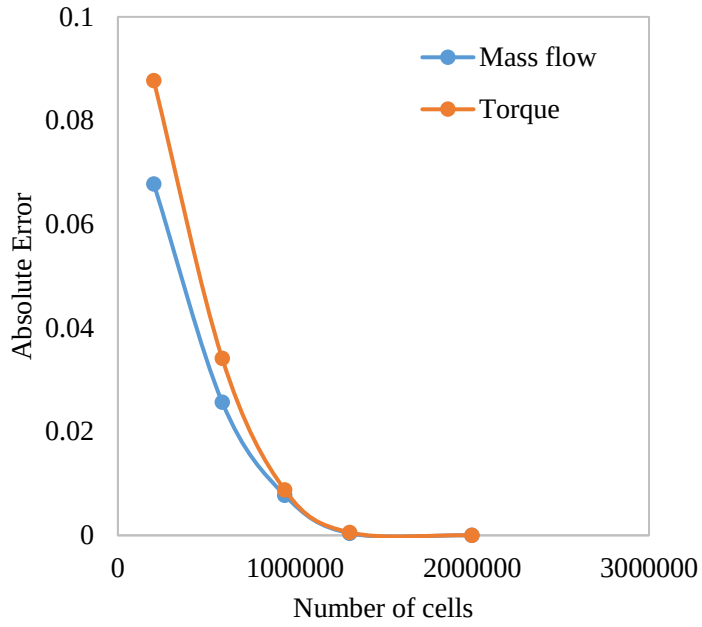

FIGURE 3: MESH CONVERGENCE FOR MASS FLOW AND TORQUE

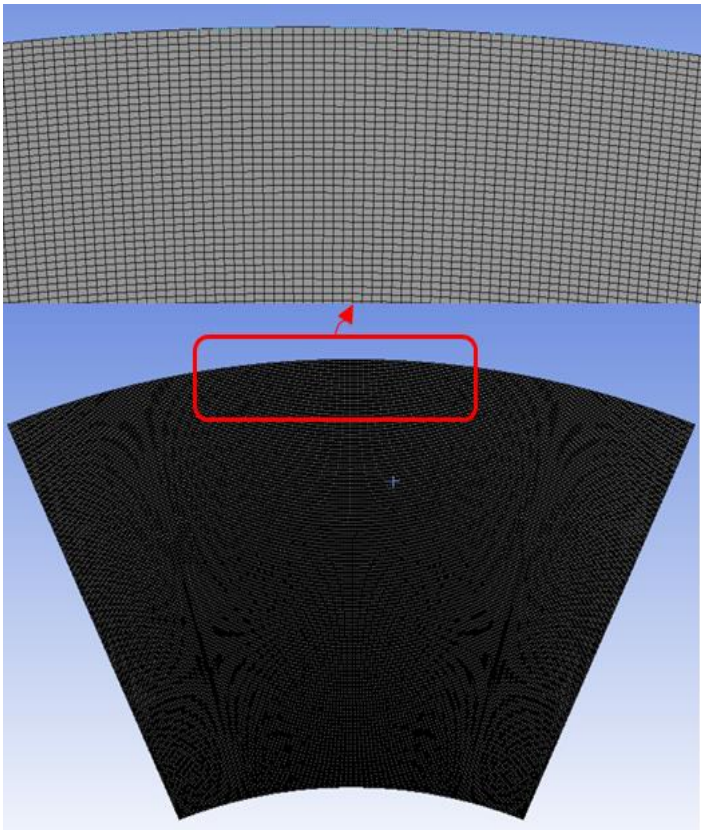

FIGURE 4a: GENERATED MESH: ROTOR ONLY ANALYSIS

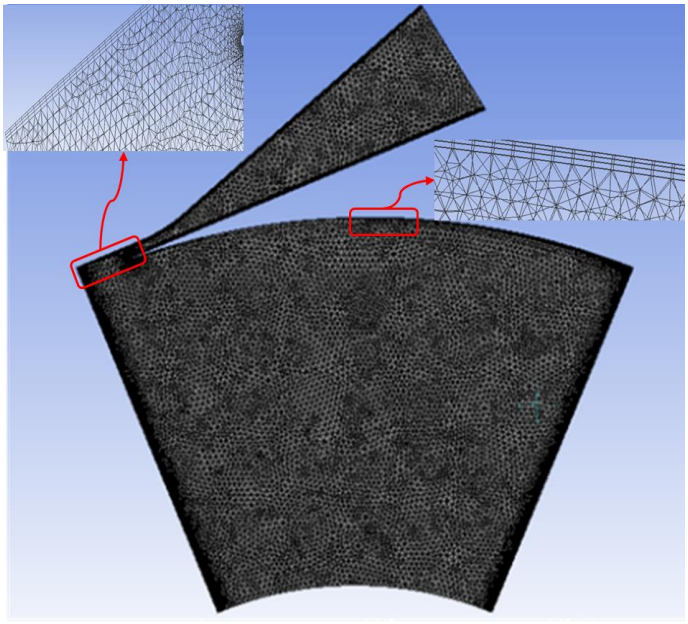

FIGURE 4b: GENERATED MESH: TESLA COMPRESSOR GEOMETRY 'CASE 0'

4.3 Performance analysis

In the "rotor only" analysis, emphasis is given to total-to-total quantities. To calculate total pressure and total to total adiabatic efficiency, Eq. (4) and (5) are used. The flow parameters at the inlet and outlet are mass flow averaged in order to calculate the compressor's overall performance (Fig. 5a).

$$PR = \frac{p_{t2}}{p_{t1}} \tag{4}$$

$$\eta_{t-t} = \dot{m}\, C_P\, T_{t1} \frac{PR^{\frac{k-1}{k}} - 1}{\tau\, \omega} \tag{5}$$

Figure 5a shows the total to total and static to static pressure ratio lines for four different Ekman numbers. The characteristic line of Ekman number equal to 1.6 is higher compared to the other cases in all mass flow rates. At the same time, the total-to-total adiabatic efficiency is higher at Ekman number 1.6 (Fig. 5b). In the tested cases, the Reynolds number is around 10 (Fig. 6), almost double than optimal 5 and 6 [18, 20]. The rotor model (M1) shows the lowest efficiency of around 78% at 0.8 Ekman number. Fig. 6 shows an efficiency increase with rising the Ekman number until 1.6. Thus, the performance map clearly shows that Ekman number around 1.6 is the optimum case, especially for low mass flow rates where "rotor only" total to total efficiency is more than 82.6%. Around a 5% efficiency increase is shown between model M1(Ek-0.8) and rotor model M3 (Ek-1.6). The static-static pressure vs mass flow is shown in Fig.5a where Ekman 1.6 indicates a higher static pressure ratio of 1.29 compared to other Ekman numbers at 0.045 g/s. The analysis is carried out for the single gap and the higher efficiency is obtained at 0.045 g/s. Increasing the disk gap that in comparing the characteristic lines of the rotor only Tesla

compressor to the conventional one, there is a different behavior. It is apparent that in our case, the pressure ratio line is asymptotic to the y-axis while in the bladed compressor is asymptotic to the x-axis. This outcome is quite interesting and it actually explains the advantage of bladeless turbomachinery. Due to the lack of blades, the flow can adapt to the optimal flow angle at different mass flow rates, giving each time the highest performance. This obviously cannot happen in a constant blade compressor where losses decrease the performance as we diverge from the operating point.

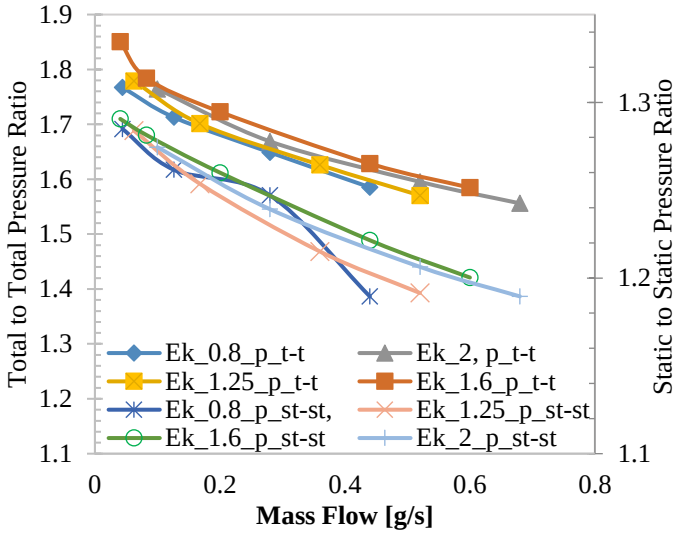

FIGURE 5 (a): ROTOR ONLY TOTAL - TOTAL AND STATIC-STATIC PRESSURE RATIO VS MASS FLOW RATE FOR DIFFERENT EKMAN NUMBERS

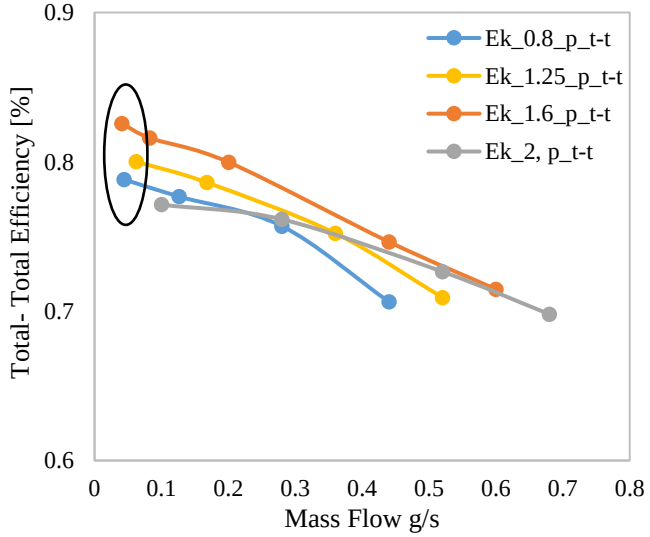

FIGURE 5(b): ROTOR ONLY TOTAL TO TOTAL ADIABATIC EFFICIENCY VS MASS FLOW RATE FOR DIFFERENT EKMAN NUMBERS

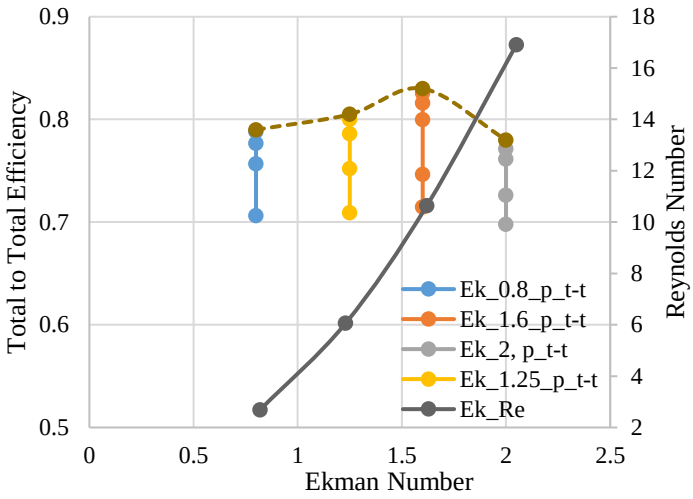

FIGURE 6: ROTOR ONLY TOTAL TO TOTAL ADIABATIC EFFICIENCY AND REYNOLDS NUMBER VS EKMAN NUMBER (Ek-0.8 -1.6 WROST- BEST AND Ek1.6-2 - BEST WROST)

Based on the numerical analysis, the flow angle is calculated to be equal to 89.88deg Eq. (6) at 0.045 g/s mass flow rate, where the total to isentropic efficiency is 82.6%. Wang [12] is calculated the flow angle at 89.5deg where isentropic efficiency is 83%.

$$\tan(\alpha_2) = \frac{V_{t2}}{V_{r2}} \tag{6}$$

For an insight into the main flow phenomena, Ekman numbers of 0.8 and 1.6 are chosen as the worst and the best cases. In both cases (fig. 7 and fig. 8), the smooth increase of the total pressure can be observed, however, the higher Ekman number case shows a higher gradient. This means momentum can be transferred more effectively to the flow in this case.

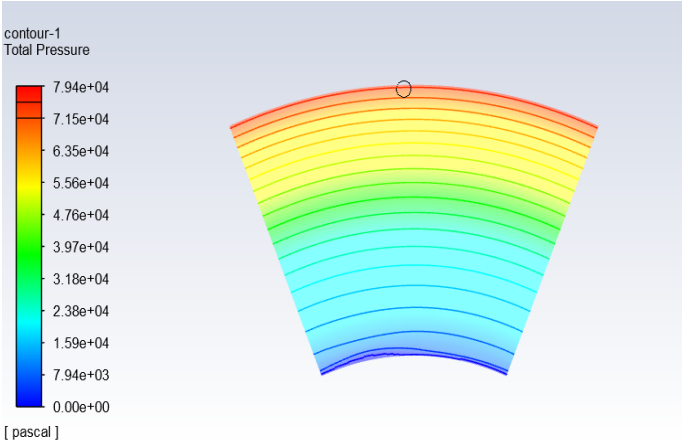

FIGURE 7: ROTOR ONLY TOTAL PRESSURE CONTOUR FOR EKMAN NUMBER = 0.8 - GAP = 0.1mm, MASS FLOW = 0.045 g/s.

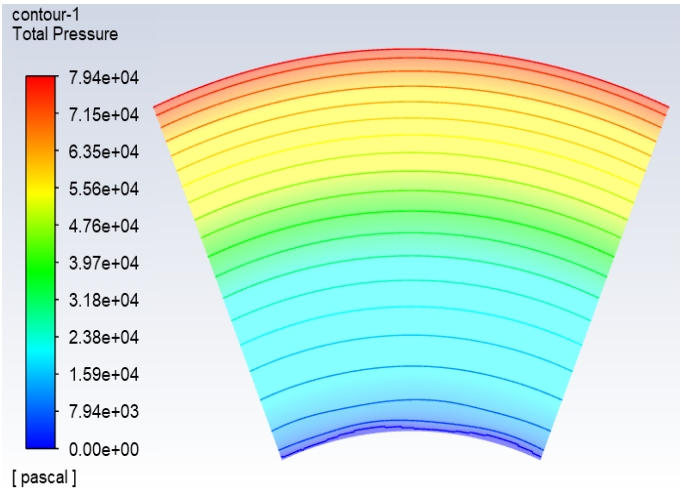

FIGURE 8: ROTOR ONLY TOTAL PRESSURE CONTOUR FOR EKMAN NUMBER = 1.6 - GAP = 0.2mm, MASS FLOW = 0.045 g/s.

5. DIFFUSER DESIGN

There are several challenges in designing the Tesla compressor to improve its performance. The stator design is quite significant and is affected by a number of parameters i.e. diffuser angle, shape, diffuser length, area ratio, clearance between diffuser and rotor. There is no specific data available to design the Tesla compressor stator. According to Rice [14], the stator/diffuser needs to be placed in a direction almost tangential to the rotor disks. However, this has not been proven yet. It is recognized that in bladeless machinery significant losses occur in the interaction [12].

In this section, starting from the original "case 0" geometry of the stator and two new diffuser configurations cases 1 and 2 are proposed as shown in table 2. The rotor-stator interaction gab is in average 0.5mm, it is the same for all tested cases and it is not an optimization parameter for this study. Furthermore, only the rectangular diffuser type is considered. In "case 0", the diffuser has an area ratio of 10.2 with a divergent angle of 18.5° while the diffuser is placed at a 2.3° angle, as shown in Fig. 2d. In "case 1", the diffuser is a bent channel with an area ratio of 3.6 where the throat is 1.3mm. The diffuser is placed at a 5 deg angle and its upper and lower sections are diverted by 2.6° and 5.6° respectively as shown in fig. 9. The second proposed (case 2) diffuser is a straight channel with a throat of 1.1mm, an area ratio of 2.7, a diffuser angle of 3.5°and a divergent angle of 2.4° (Fig. 10). The width is kept the same in all diffuser cases. According to standard maps for a linear diffuser with a rectangular cross-section [19,22], the "case 0" diffuser lies outside, which shows the recirculation as visualized in Fig 13(b). This diffuser was designed for the expander model; hence an improved design of the diffuser is needed. The "case 1" and "case 2" diffusers are fulfilling the requirement of standard linear diffuser maps and increase the performance of the compressor. Based on the literature, the second proposed diffuser configuration (case 2) is expected to have better performance due to the higher-pressure recovery [19].

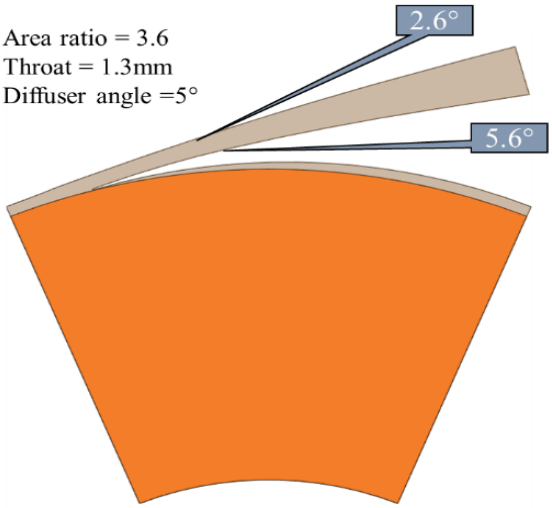

FIGURE 9: PROPOSED DIFFUSER CASE 1 WITH ROTOR MODEL M3(Ek-1.6)

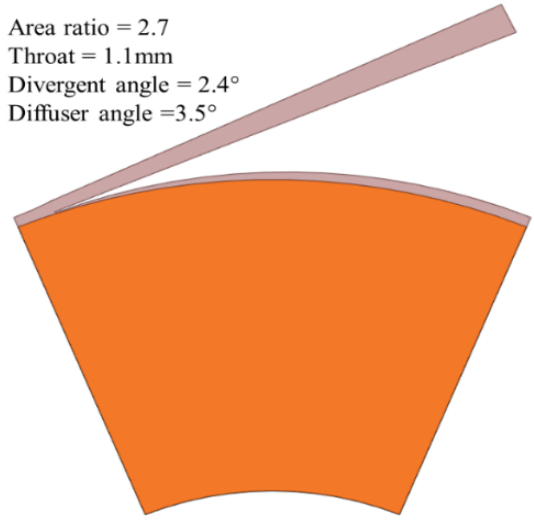

FIGURE 10: PROPOSED DIFFUSER CASE 2 WITH ROTOR MODEL M3 (Ek-1.6)

TABLE 2: DESIGN PARAMETERS OF DIFFUSER

Model	No. of diff	Throat (mm)	Exit (mm)	Length (mm)	Diff angle (°)	Divergent angle (°)
Case 0	8	1.0	10.2	31	2.3	18.5
Case 1	8	1.31	4.76	40	5	4*
Case 2	8	1.1	3.0	45	3.5	2.4

6. RESULTS

The combination of rotor-diffuser configuration is simulated at a rotational speed of 40 krpm. First, the "case 0" model of the Tesla expander running in reverse mode is assessed, aligned with the original prototype. Then, the same rotor, operated in reverse rotational speed and coupled alternatively to one of the two new diffusers, is numerically investigated. The simulation is steady-

state, and the performance characteristics are calculated based on mass flow averaged numerical results at the inlet/outlet of the Tesla compressor.

Fig 11 presents the total to static pressure ratio as a function of mass flow rate for the three diffuser configurations (Cases 0,1 and 2). Pressure ratio decreases with the mass flow increase as expected, the rotor model M3 (Ek-1.6) presents the highest static to static 1.29 and total to total 1.85 pressure ratio at low mass flow 0.045 g/s as shown in Fig. 5b, where rotor efficiency is 82.6%. The total-static pressure ratio obtained for "case 2" is 1.45. However, the characteristic curve of the Tesla compressor with the second proposed diffuser "case 2" shows higher pressure ratios compared to other configurations. The better performance is achieved at a low mass flow rate for all three diffuser configurations. It is quite important to mention the drop of the pressure ratio due to the existence of the diffuser. Rotor only analysis shows that the total to total pressure ratio can reach up to 1.8 at low at mass flow for model M3 (E_k =1.6, gap 0.2). M3 model tested with both proposed diffusers cases 1 & 2, and total to static pressure ratio found 1.41 for the first diffuser "case 1" and 1.45 for the second "case 2" at the mass flow rate of 0.045g/s (Fig. 11). The overall analysis is carried out based on the single disk gap.

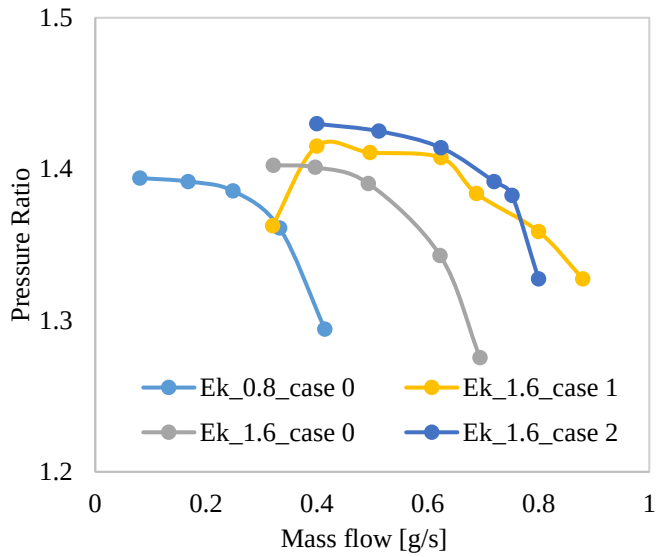

FIGURE 11: TOTAL - STATIC PRESSURE RATIO VS MASS FLOW RATE FOR DIFFERENT COMPRESSOR CONFIGURATIONS

Apart from the pressure ratio, total to static efficiency is also calculated for the "rotor-diffuser" configurations. Fig. 12 presents the produced results, the efficiency curve of the "case 2" diffuser stands out compared to the other two cases 0 & 1. Maximum efficiency appears at 0.4 g/s and is 53% for the case 2 diffuser-rotor model (M3-Ekman 1.6) The case 0 configuration has again the lowest efficiency while the first configuration floats between the rest. Considering the model (M1) of rotor only analysis, the total to total efficiency at 0.4 g/s is 70.6%, while Model M3 is 75%.

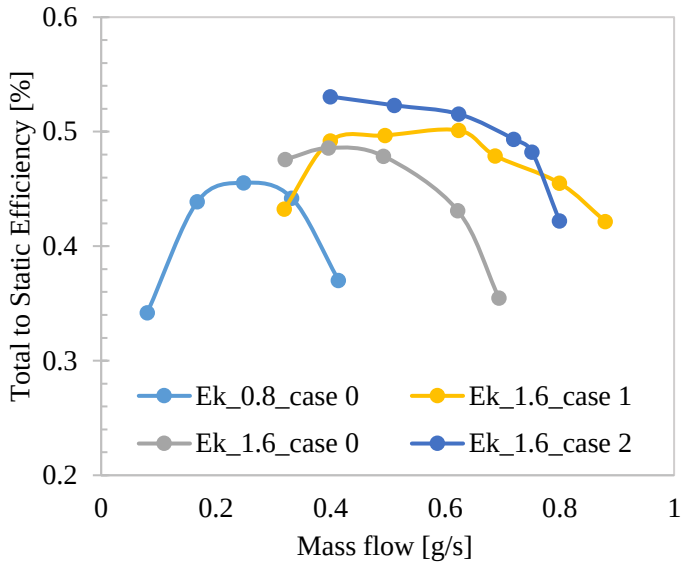

FIGURE 12: TOTAL TO STATIC EFFICIENCY VS MASS FLOW RATE FOR DIFFERENT COMPRESSOR CONFIGURATIONS

Having a closer observation on the computational fluid dynamic results and specifically on the static pressure and velocity contours in Fig. 13-14, the shape of the performance line can be explained. With regards to the case 0 configuration, a massive recirculation area appears at the exit of the diffuser. The diffuser divergence angle is way far from the ideal values, making the flow to separate. The second diffuser has a better performance. Its wall angles are in the optimum design range. However, at the exit of the first diffuser configuration, a jet-wake flow is observed. Moreover, the area covered by the wake flow is almost the same as the area of the jet. The absence of a separation bubble makes that configuration better than the case 0. Fig. 13 (a & b) shows the static pressure and velocity fields of the best-tested configuration at 0.49 g/s mass flow. The diffuser design must have a direct impact on the performance characteristics of the Tesla compressor. The "Case 0" shows a huge recirculation in the diffuser which is minimized in case 1 and further minimize in case 2 diffuser as shown in Fig. 14 a & b. Fig 14 b shows the velocity differences in the upper and lower region at the exit of the diffuser. The velocity field at the exit of the diffuser is more uniform, limiting the separation losses. A reduced area of wake flow still exists at the top wall of the diffuser. However, this is because of the velocity profile entering the diffuser. The upper and the lower walls of the diffuser are located at different radii, thus, the profile is not constant, resulting in the confined jet-wake outlet profile. The implementation of model M3 (Ek-1.6) will benefit in the overall performance and reduce the number of disks by 33% as shown in table 1 and as a result the production cost.

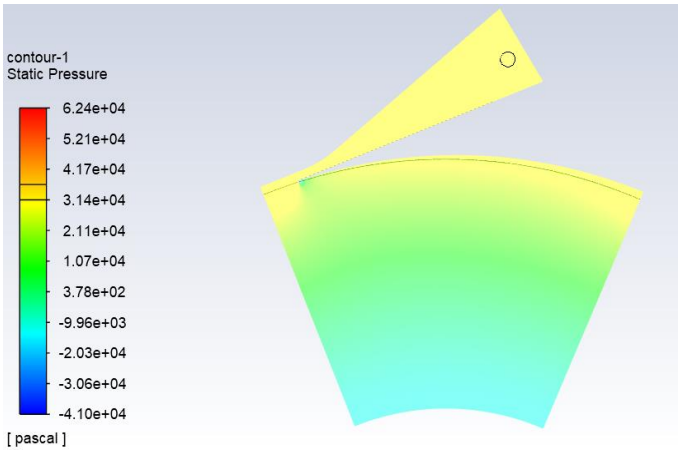

FIGURE 13a: STATIC PRESSURE CONTOURS FOR CASE 0 PROTOTYPE GEOMETRY (EK-1.6, MASS FLOW-0.49 g/s)

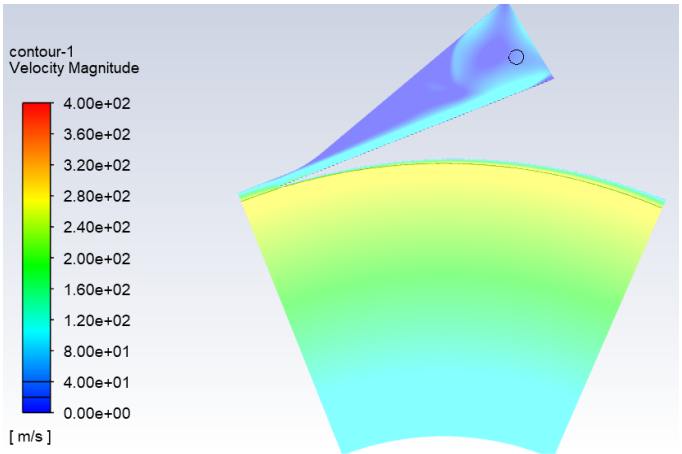

FIGURE 13b: VELOCITY CONTOURS FOR CASE 0 PROTOTYPE GEOMETRY (CASE 0, EK-1.6, MASS FLOW-0.49 g/s)

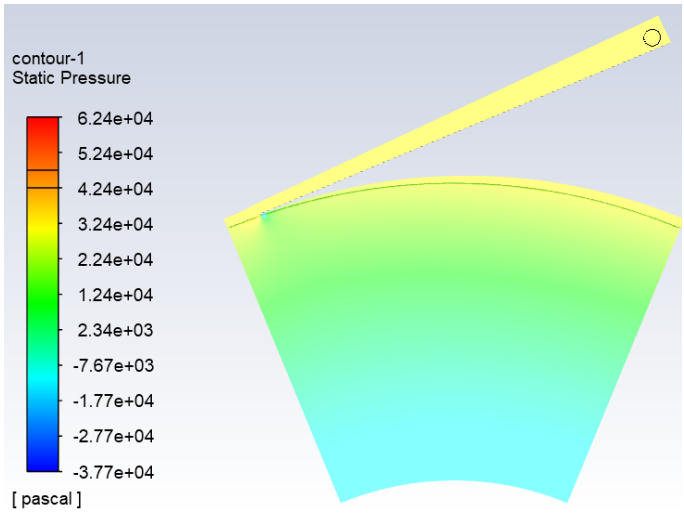

FIGURE 14a: STATIC PRESSURE FOR PROPOSED DIFFUSER (CASE 2, EK-1.6, MASS FLOW = 0.49 g/s)

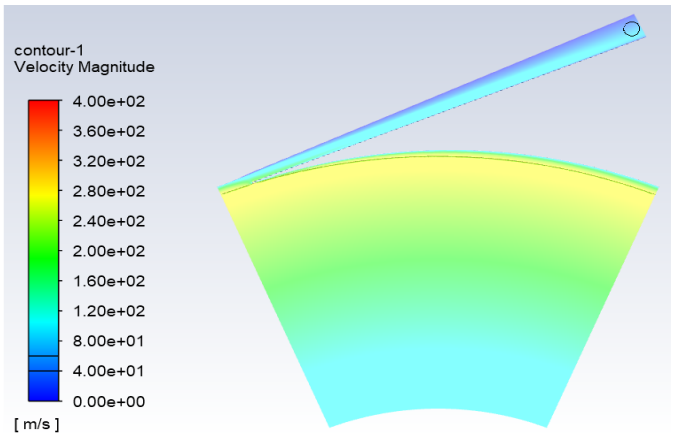

FIGURE 14b: VELOCITY CONTOURS FOR PROPOSED DIFFUSER (CASE 2, EK-1.6, MASS FLOW = 0.49 g/s)

7. CONCLUSION

This paper investigates numerically the performance of the Tesla compressor based on a case 0 prototype geometry by analyzing the flow phenomena between two corotating disks. First, an independent rotor analysis investigates the optimum Ekman number for maximum performance. Afterward, two different diffuser shapes are proposed. And finally, three rotor-diffuser configurations are numerically tested, and their results were compared with the outputs of the "rotor only" analysis. The following main results are found in the present study:

- The rotor only analysis shows that the axial distance between two disks significantly affects the performance of the Tesla compressor: peak performance is found an Ekman number 1.6, while optimal Reynolds number is 10.
- A new characteristic line shape of the rotor only test is found, due to self-corrected flow angle of the fluid.
- The rotor model M3 showed the highest rotor efficiency more than 82.5%. This is 5% higher than the "case 0" rotor model M1, and if we replace the model M1 with M3, 33% of the total disk and gap would be reduced in "case 0" prototype model.
- The rotor-stator computational analysis reveals that in order to use a Tesla turbine in reverse mode (as Tesla compressor), the diffuser needs to be modified. Moreover, results show that the second proposed diffuser "case-2" configuration has better performance in total to static and static to static pressure ratio. The overall efficiency obtained 53% at 0.40 g/s mass flow for the M3 rotor model, while rotor model M1 "case 0" diffuser is 36% at 0.40 g/s.
- The non-uniform velocity profile at the inlet of the diffuser directly affects the performance of the diffuser and the performance of the whole Tesla compressor.

ACKNOWLEDGEMENTS

This project has received funding from the European Union's Horizon 2020 research and innovation programme under the Marie Skłodowska-Curie grant agreement No 861079.

REFERENCES

[1] Tesla, N., 1913, “Turbine”, US Patent 1061206.

[2] Tesla, N., 1913, “Fluid propulsion” US Patent 1061142.

[3] Rice, W., 1965, “An Analytical and Experimental Investigation of Multiple Disk Turbines”,. Journal of Engineering for Power, Vol. 87(1), pp. 29–36.

[4] Lemma, E., Deam, R., Toncich, D. & Collins, R., 2008, “Characterisation of a small viscous flow turbine”, Experimental Thermal and Fluid Science, 33(1), pp. 96-105.

[5] Epstein, A. H., 2004, “Millimeter-Scale, Micro-Electro-Mechanical Systems Gas Turbine Engines”, ASME J Eng Gas Turbines Power, 126(2), pp. 205-226.

[6] Renuke, A, F. Reggio, P. Silvestri, A. Traverso, M. Pascenti, 2020 “Experimental Investigation on a 3 kW Air Tesla Expander With High-Speed Generator”, ASME Paper GT2020-14572, ASME Turbo Expo 2020, virtual.

[7] Beans, E. W., 1961, “Performance Characteristics of a Friction Disk Turbine,” Ph.D thesis, The Pennsylvania State University, State College, PA.

[8] Sirakov, B. T., Gong, Y., Epstein, A. H., and Tan, C. S., 2004, “Design and Characterization of Micro-Compressor Impellers,” ASME Paper No. GT2004-53332.

[9] Laroche, E., and Ribaud, Y., 1999, “An Analysis of the Internal Aerodynamic Losses Produced in the Laminar and Centrifugal Flow Between Two Parallel Co-rotating Disks,” Proc. 3rd European Conference on Turbomachinery-Fluid Dynamics and Thermodynamics, IMechE Event Publications, London, Paper No. C557/001/99.

[10] Crawford, M. E., and Rice, W., 1974, “Calculated Design Data for the Multiple-Disk Pump Using Incompressible Fluid” ASME J.Eng. Power, 96(3), pp. 274–282.

[11] Boyd, K. E., and Rice, W., 1968, “Laminar Inward Flow of an Incompressible Fluid Between Rotating Disks With Full Peripheral Admission,” ASME J. Appl. Mech., 90(2), pp. 229–237.

[12] Wang, B., Okamoto, K., Yamaguchi, K. and Teramoto, S., 2014, “Loss mechanisms in Shear-Force Pump with Multiple Corotating Disks” ASME J. Fluids Eng., 136(8).

[13] Breiter, M. C., and Pohlhausen, K., 1962, “Laminar Flow Between Two Parallel Rotating Disks,” Aeronautical Research Laboratories, Wright-Patterson Air Force Base, OH, Technical Report No. ARL 62-318.

[14] Rice, W., 1963, “An Analytical and Experimental Investigation of Multiple Disk Pumps and Compressors,” ASME J. Eng. Power, 85(3), pp, 191–199.

[15] Boyack, K. E., and Rice, W., 1971, “Integral Method for Flow Between Corotating Disks,” ASME J. Basic Eng., 93(3), pp. 350–354.

[16] Brett Dewar, Mike Creamer, 2019, “CFD Modelling of a Centrifugal Compressor with Experimental Validation through Radial Diffuser Static Pressure Measurement”, Hindawi International Journal of Rotating Machinery Volume 2019, Article ID 7415263, 12 pages. https://doi.org/10.1155/2019/7415263.

[17] Hasinger, S. H., and Kehrt, L. G., 1963, “Investigation of a Shear Force Pump,” ASME J. Eng. Power, 85, pp. 191–198.

[18] Rice, W., 2003, “Tesla Turbomachinery,” Handbook of Turbomachinery, Logan, E., and Ray, R., Marcel Dekker, New York, Chap. 14.

[19] Schmandt, Bastian & Herwig, Heinz. (2011), “Diffuser and Nozzle Design Optimization by Entropy Generation Minimization. Entropy”, 13, 1380-1402, 10.3390/e13071380.

[20] Oliveira D. C. M., 2009, “Analytical and experimental modeling of a viscous disk pump for MEMS applications” III Conferência Nacional em Mecânica de Fluidos, Termodinâmica e Energia (MEFTE - BRAGANÇA)

[21] Abo Elyamin, 2019, “Effect Of Impeller Blades Number on The Performance of a Centrifugal Pump” Alexandria Engineering Journal (2019) 58, 39–48.

[22] Shigeru Obayashi, Shinkyu Jeong and Koji Shimoyama,2010 “Multi-Objective Design Exploration and its Applications” Int’l J. of Aeronautical & Space Sci. 11(4), 247–265 (2010) DOI:10.5139/IJASS.2010.11.4.247.

[23] Zhu, Y.; Jiang, P., “Experimental and numerical investigation of the effect of shock wave characteristics on the ejector performance”. Int. J. Refrig. 2014, 40, 31–42.

[24] Croquer, S., Poncet, S., Aidoun, Z., “Turbulence modeling of a single-phase R134a supersonic ejector. Part 1: Numerical benchmark”. Int. J. Refrig. 2016, 61, 140–152.

[25] J. Galindo, S. Hoyas, P. Fajardo & R. Navarro, 2013 “Set-Up Analysis and Optimization of CFD Simulations for Radial Turbines”, Engineering Applications of Computational Fluid Mechanics, 7:4, 441-460, DOI: 10.1080/19942060.2013.11015484.

[26] Menter FR, 1992, “Influence of freestream values on k-omega turbulence model predictions”. AIAA journal 30:1657-1659.